



Development and characterization of a Versatile Engineered Nanomaterial Generation System (VENGES) suitable for toxicological studies

Citation

Demokritou, Philip, Robert Büchel, Ramon M. Molina, Glen M. Deloid, Joseph D. Brain, and Sotiris E. Pratsinis. 2010. "Development and Characterization of a Versatile Engineered Nanomaterial Generation System (VENGES) Suitable for Toxicological Studies." *Inhalation Toxicology* 22 (sup2) (August 11): 107–116. doi:10.3109/08958378.2010.499385.

Published version

<https://doi.org/10.3109/08958378.2010.499385>

Link

<http://nrs.harvard.edu/urn-3:HUL.InstRepos:30085133>

Terms of use

This article was downloaded from Harvard University's DASH repository, and is made available under the terms and conditions applicable to Other Posted Material (LAA), as set forth at

<https://harvardwiki.atlassian.net/wiki/external/NGY5NDE4ZjgzNTc5NDQzMGIzZWZhMGFIOWI2M2EwYTg>

Accessibility

<https://accessibility.huit.harvard.edu/digital-accessibility-policy>

Share Your Story

The Harvard community has made this article openly available.
Please share how this access benefits you. [Submit a story](#)



HHS Public Access

Author manuscript

Inhal Toxicol. Author manuscript; available in PMC 2015 May 08.

Published in final edited form as:

Inhal Toxicol. 2010 December ; 22(0 2): 107–116. doi:10.3109/08958378.2010.499385.

Development and characterization of a Versatile Engineered Nanomaterial Generation System (VENGES) suitable for toxicological studies

Philip Demokritou^{c,*}, Robert Büchel^a, Ramon M. Molina^b, Glen M. Deloid^b, Joseph D. Brain^b, and Sotiris E. Pratsinis^a

^aParticle Technology Laboratory, Department of Mechanical and Process Engineering, ETH Zurich, Sonneggstrasse 3, CH-8092 Zurich, Switzerland ^bMolecular and Integrative Physiological Sciences, Department of Environmental Health, Harvard School of Public Health, 665 Huntington Avenue, Boston, MA 02115, USA ^cExposure Epidemiology and Risk Program, Department of Environmental Health, Harvard School of Public Health, 401 Park Drive, Landmark Center, Boston, MA 02215, USA

Abstract

A novel system for generation of engineered nanomaterials suitable for *in situ* toxicological characterization within biological matrices was developed. This Versatile Engineered Nanomaterial Generation System (VENGES) is based on industry-relevant, flame spray pyrolysis (FSP) aerosol reactors that can scaleably produce engineered nanomaterials (ENMs) with controlled primary and aggregate particle size, crystallinity and morphology. ENMs are produced continuously in the gas phase, allowing their continuous transfer to inhalation chambers, without altering their state of agglomeration. Freshly generated ENMs are also collected on Teflon filters for subsequent physico-chemical and morphological characterization and for *in vitro* toxicological studies.

The ability of the VENGES system to generate families of ENMs of pure and selected mixtures of iron oxide, silica and nanosilver with controlled physico-chemical properties was demonstrated using a range of state-of-the-art-techniques. Specific surface area was measured by nitrogen adsorption using the Brunauer-Emmett-Teller (BET) method, and crystallinity was characterized by X-ray diffraction (XRD). Particle morphology and size were evaluated by scanning and transmission electron microscopy (*STEM/TEM*). The suitability of the VENGES system for toxicological studies was also shown in both *in vivo* and *in vitro* studies involving Sprague-Dawley rats and human alveolar-like monocyte derived macrophages, respectively. We demonstrated linkage between physico-chemical ENM properties and potential toxicity.

*Corresponding Author: Philip Demokritou, Ph.D. Department of Environmental Health, School of Public Health, Harvard University, 401 Park Drive, BOX 15677, Landmark Center- West, Boston, MA 02215, USA, Tel: (617) 3848847, pdemokri@hsph.harvard.edu.

Keywords

Engineered nanomaterials; *in vivo* inhalation studies; *in vitro* toxicological studies; iron oxide; silica; nanosilver

Introduction

The global nanotechnology industry will increase exponentially to a \$1 trillion business by 2015 (Aitken et al., 2006). The release of engineered nanomaterials (ENMs) into the environment during manufacture and use appears to be an inevitable consequence of their increasingly widespread use in numerous applications and commercial products as diverse as medical devices, drug delivery, cosmetics and textiles (Nel et al., 2009). Workers who manufacture, package, transport, and utilize ENMs, as well as the general public, might be exposed to ENMs through multiple routes.

There is growing evidence that supports the potential for ENMs to cause biological effects (Colvin, 2003; Service, 2000; Nel et al., 2006; Brain et al., 2009). Indeed, we know that many small particles and fibers cause lung injury and inflammation at high doses (Brain et al., 1994). Moreover, the potential of nanoparticles and nanofibers to translocate through the air-blood barrier, and thus to reach the pulmonary connective tissues, lymphatic system, or even the circulating blood, and thence have access to other critical organs, is of great concern (Nel et al., 2009, 2006). An important indicator of danger is persistence of materials in the lungs (Brain et al., 1994). Those that rapidly dissolve and disappear are less hazardous than those that accumulate and persist in the lungs. We therefore need to characterize the biopersistence of ENMs.

Potential toxicity and environmental effects are critical factors in the likely success or failure of novel nanotechnologies. As outlined in the most recent US National Nanotechnology Initiative report and the National Research Council's recent review of the Federal Government strategy on nanotechnology, it is a high priority to develop novel ENM generation systems that can be used for the *in situ* characterization of ENMs within biological matrices (National Science and Technology Committee, 2008; NRC, 2008). Such systems must have the ability to generate industry-relevant ENMs, while controlling their physico-chemical and morphological properties, as dictated by requirements for specific functional applications. The coupling of these systems with the development and use of new *in vitro* and *in vivo* toxicological assays will help to identify which physico-chemical properties of ENMs correlate best with biological interactions.

Two main methods are employed in the nanotechnology industry to produce families of metal oxide nanomaterials: dry aerosol and wet chemistry technologies (Mukhopadhyay and Basu, 2007; Wegner and Pratsinis, 2003a). Flame-made nanostructured materials account for over 90% of the current global production volume and value of aerosol-made ENMs (Wegner and Pratsinis, 2003a), such as carbon blacks, silica and pigmentary titania. These nanomaterials are already industrial commodities manufactured worldwide at a rate of tons per hour (Ulrich, 1984). Flame reactors are preferred over conventional wet technologies, especially for large scale manufacture of particles, because they a) do not create liquid by-

products requiring costly cleaning, b) offer easier collection of particles (i.e. from gases rather than liquids), c) involve fewer process steps, d) form high purity products (e.g., optical fibers), e) have unique filamentary morphology (fumed silica and carbon black) that is attractive for production of nanocomposites (e.g. silicones and tires), and f) contribute to stable synthesis of metastable materials, such as epsilon-WO₃ for diabetes detection by human breath analysis (Righettoni et al., 2010), and low-temperature BaCO₃ for NO_x abatement by catalytic storage-reduction (Strobel and Pratsinis, 2007).

A breakthrough in flame technology was achieved with the systematic development of liquid-fed flame aerosol reactors (Madler et al., 2002a), the so-called Flame Spray Pyrolysis (FSP) reactors, which are distinguished by their flexibility in producing functional materials of various compositions and morphologies. These sophisticated FSP generated nanostructured materials have broad applications in the production of diverse products such as catalysts, gas sensors, phosphors, fuel cells, batteries, dental and orthopedic materials, and even nutritional supplements (Strobel and Pratsinis, 2007), as well as durable sorbents for CO₂ sequestration (Lu et al., 2009).

The simplicity and robustness of flame reactors (no moving parts) result in their minimal maintenance, facilitating continuous production of materials, such as carbon black, silica, alumina and titania today. This, coupled with the current understanding of relationships between flame process parameters and product characteristics, permits the manipulation and precise control of particle properties (Pratsinis, 1998). These process features are crucial for large scale synthesis of novel materials with superior performance. Such materials are typically composed of solid or hollow primary particles (Strobel and Pratsinis, 2007), fractal-like aggregates (particles held together by chemical or sinter bonds) and agglomerates (particles held together by physical bonds such as Van der Waals forces) (Tsantilis and Pratsinis, 2004). The sizes of constituent structures may range from nanometer-sized primary particles to micron-sized agglomerates. The characteristics, and therefore the performance, of flame-made particles are controlled by the burner configuration and precursor composition. They determine the synthesis temperature, as well as the composition and structure of the ENMs (Pratsinis, 1998). Short residence times in the flame region and faster cooling rates reduce primary particle size and extent of aggregation (Tsantilis and Pratsinis, 2004; Teleki et al., 2008a). Even faster quenching can be achieved by injecting cold air or O₂, or by expanding the flame through a supercritical nozzle (Wegner and Pratsinis, 2003b). In addition, nanoparticle surfaces may be coated (Teleki et al., 2005) to improve dispersion (Teleki et al., 2008b) in liquid suspensions (e.g., inks, paints, wafer polishing slurries) or in polymers (e.g., dental prosthetics, tires, toothpaste).

Here we report the development and characterization of a FSP-based, ENM generation system suitable for *in vivo* and *in vitro* toxicological studies. This system is based on industry-relevant, FSP aerosol reactors with the capacity to scaleably produce nanomaterials with closely controlled primary particle and aggregate sizes, crystallinity and morphology. ENMs are produced continuously in the gas phase, allowing their controlled transfer, with a low agglomeration state, to inhalation chambers. ENMs are also collected on Teflon filters, from which they can be extracted as powders for physico-chemical and morphological characterization, and for *in vitro* toxicological studies. Three ENMs were selected and

generated for performance characterization: iron oxide, silicon dioxide (SiO₂) and nanosilver supported on SiO₂. The physico-chemical and morphological properties of particles were characterized by nitrogen adsorption (BET), X-ray diffraction (XRD), and scanning and transmission electron microscopy (STEM/TEM). The suitability of the VENGES system for toxicological characterization studies was also demonstrated in preliminary experiments involving exposure of Sprague-Dawley rats and human alveolar-like monocyte derived macrophages to different generated ENMs.

Methods

Experimental setup

Figure 1 illustrates the Versatile Engineered Nanomaterial Generation System (VENGES). The system consists of three main components: ENM synthesis; Particle sampling and collection system; and Animal exposure system.

ENM synthesis—The synthesis of ENMs is based on the industry-relevant FSP method. A schematic of the setup (Tethis, NPS 10) is shown in Figure 1. An inflammable liquid precursor, containing dissolved organometallic compounds, is pumped through a stainless-steel capillary tube (ID 0.41 mm; OD 0.71 mm). Immediately surrounding the capillary tube is a narrow annular gap of adjustable cross-sectional area that supplies a flow of oxygen, which is used to disperse the liquid precursor into fine droplets. A small pilot flamelet (premixed CH₄ and O₂ at 1 and 2 L/min, respectively) ignites the droplets so that the organic parts of the precursor combust, while the metals are oxidized, and form particles that grow by coagulation and sintering in the flame. The precursor liquid feed is metered by a mass rate-controlled syringe pump, and all gas flows are controlled using mass flow controllers. Further details of the apparatus are given in Madler et al. (2002a) and Teleki et al. (2008a).

Particle sampling and collection system—The flame-generated particles are collected using a water-cooled, stainless-steel filter housing supporting a glass fiber filter (Whatman GF6, 25.7 cm in diameter), with exhaust gases drawn by a vacuum pump (Busch, Seco SV 1040C). Collected particles can be extracted from the filter as powder, and used for off-line physico-chemical and morphological characterization, as well as for *in vitro* or *in vivo* toxicological studies.

Animal exposure system—The continuously produced (in the gas phase) nanoparticles may be sampled *in situ* over the flame, and transferred to inhalation chambers for animal studies. Freshly generated ENMs are sampled at an adjustable flow rate (0.3 - 1 L/min), and immediately diluted with HEPA-filtered dry air using a rotating disk dilutor (TSI, model 379020A). The diluted ENMs remain airborne, with very low levels of agglomeration, and may be drawn directly through animal exposure chambers (Figure 1).

VENGES performance characterization

Experiments were performed to investigate VENGES's ability to generate ENMs with closely controlled physico-chemical characteristics (size, composition and morphology).

Three ENMs were selected for these performance characterization experiments: iron oxide, silica dioxide and nanosilver. These materials were selected for their unique properties, and for their current and promising applications. Iron oxides have crystalline structure, and have magnetic and superparamagnetic properties that make them attractive in biomedical, and even nutritional, applications (Teleki et al., 2009; Hilty et al., 2009), and are used as such in a variety of popular commercial products. Silica nanoparticles have an amorphous structure, and are the fourth largest aerosol-made materials, with a multitude of applications, including aiding flow, cosmetics, pharmaceuticals and varnishes (Ulrich, 1984). Finally, nanosilver has become a much-discussed nanomaterial, and has attracted the attention of US EPA because of its potential toxicity (Lubick, 2008). Table 1 summarizes the ENMs generated here, their liquid precursors, and synthesis conditions. The pressure drop of the dispersion gas over the nozzle was adjusted to 2 bar before the igniting/supporting flamelets were turned on. The pressure drop decreased slightly during production, to the value shown in Table 2.

Controlling particle size—VENGES's ability to vary particle size was tested for both iron and silicon oxide particles. Particle size was controlled by varying the O₂ dispersion flow rate between 3 and 7 L/min, and by varying the liquid precursor (fuel) flow rate from 3 to 7 mL/min. Table 2 summarizes the conditions used in the ENMs synthesis.

Reproducibility—In addition, the experiments with SiO₂ for liquid precursor to dispersing gas ratios of 3/7, 5/5 and 7/3 were repeated 3 times to test VENGES's ability to reproduce ENMs with constant particle characteristics. The average, maximum, and minimum particle sizes were measured using the particle size characterization methods described below.

Surface modification experiments—Flame generated ENMs can be surface-modified *in situ* by applying various organic (Teleki et al., 2010) or inorganic (e.g. silica) coatings (Teleki et al., 2009 and 2008c). These surface modifications may alter toxicological properties. VENGES's ability to generate surfaced-modified particles was tested with SiO₂-based nanoparticles. Here, their surface was modified by depositing on it various mass fractions of nanosilver (1, 5, 10 and 99 Ag wt%, Table 1). Because SiO₂ and Ag have different melting points, silica forms first, acting as a nucleation seed for the Ag nanoparticles, which adhere to its surface. For Ag/SiO₂ synthesis the 5/5 FSP liquid precursor/dispersing gas flow ratio was chosen.

ENM characterization

Specific surface area and primary particle size—Total surface area was measured with a 5-point nitrogen adsorption isotherm at 77 K (Micrometrics Tristar), using the BET method. The specific surface area (SSA) is defined as the area per mass (m²/g). Assuming spherical particles, with a surface area of πd_{BET}^2 , and a mass of $\pi d_{BET}^3 \rho_p / 6$, the equivalent primary particle diameter (d_{BET}) is:

$$d_{BET} = 6 / (SSA \cdot \rho_p) \quad (1)$$

with ρ_p being the particle density (4.79 g/cm³ for γ -Fe₂O₃, 2.2 g/cm³ for SiO₂, and a composite value depending upon Ag wt% for Ag/SiO₂). The d_{BET} diameter is often referred to as the primary particle size, as all individual particles in an aggregate/agglomerate contribute to the total surface area.

Crystallinity—X-ray diffraction (XRD) patterns were recorded (Bruker D8 Advance, 40 kV, 40 mA, $\lambda = 1.54$ nm) at a scan speed of 0.5°/min at $10^\circ < 2\theta < 70^\circ$. The crystal size (d_{XRD}) was calculated from the line broadening of the spectra using the fundamental parameter approach and the Rietveld method. The d_{XRD} represents the average diameter of the crystalline part.

Morphology—Collected ENM samples were sent to the Harvard Center for Nanoscale Systems (CNS) for scanning transmission electron microscopy (STEM) analysis. Samples were also analyzed at ETH Zurich by transmission electron microscopy (TEM).

For scanning transmission electron microscopy (STEM), the samples were dispersed in ethyl alcohol and deposited onto ultra-thin holy-carbon foil supported on a copper grid (Ted Pella Inc). Images were obtained with a high-angle annular dark-field (HAADF) detector attached to a Zeiss Libra Cs STEM (Zeiss, Monochromated, Aberration-Corrected STEM, Cs=-1 μ m), showing the metal particles with bright contrast (Z contrast). For TEM imaging, samples were dispersed in ethanol and deposited onto a perforated carbon foil supported on a copper grid (Okenshoji Co., Ltd.), and analyzed on a Philips CM12 operated at 100 kV.

Toxicological characterization

Preliminary *in vitro* and *in vivo* toxicological studies were performed using the generated ENMs in order to explore links of basic physico-chemical properties with biological outcomes.

Animal bioassay- Intratracheal instillation study—Animal protocols used in this study were approved by the Harvard Medical Area's Animal Use Committee. Fifteen male Sprague-Dawley rats (200-225 g) were obtained from Charles River Lab (Wilmington, MA). Rats were allowed to acclimate to the animal facility for 4-5 days prior to start of experiments. The animals (5 per group) were intratracheally instilled with phosphate buffered saline (PBS) suspensions of ENMs at a mass dose of 1 mg/kg and volume dose of 1.5 ml/kg. An equivalent volume of PBS was used as a control. The dosing liquid suspension was measured in a sterile syringe with an attached blunt-tipped 18 gauge gavage needle. Rats were then anesthetized with 3% vaporized isoflurane, restrained on a slanted board, and held upright by their upper incisor teeth resting on a rubber band. The larynx was positioned under an intensely focused light source to ensure visualization during instillation. While the animals were under anesthesia, the tip of the gavage needle was gently inserted into the trachea between the vocal cords, with the tip just above the tracheal bifurcation, and the dosing suspension was delivered in one quick bolus. The animals were allowed to recover from anesthesia in slanted position while the thorax was gently massaged to facilitate distribution of the instillate throughout the lungs.

At twenty four hours post-exposure to ENMs, rats were humanely killed with isoflurane anesthesia followed by exsanguination. The trachea was exposed and cannulated, and bronchoalveolar lavages (BAL) of the lungs were done twelve times with 3 ml of Ca^{++} and Mg^{++} -free PBS. Lavaged cells were separated from the supernatant in all washes by centrifugation. Total and differential cell counts and hemoglobin measurements were made from the cell pellets. The combined acellular supernatant fractions from the first two washes was analyzed for indicators of injury and inflammation, including lactate dehydrogenase (LDH), myeloperoxidase (MPO), and albumin. This bioassay system has been described earlier (Beck et al., 1982). All BAL parameters were analyzed using analysis of variance (ANOVA) followed by Bonferroni *post hoc* analyses using SAS statistical software (Cary, NC).

Membrane integrity cytotoxicity assay—The extent of nuclear staining, within a population of cells, by the membrane-impermeant fluorescent nucleic acid dye, SYTOX Green, is a useful indicator of cytotoxicity (Langsrud and Sundheim, 1997; Roth et al., 1997). The suitability of ENMs generated by the VENGES system for *in vitro* cytotoxicity assays was tested by measuring SYTOX Green nuclear staining in cells exposed to VENGES-generated ENMs.

Human alveolar-like monocyte derived macrophages (AM-MDMs), prepared as described previously (Sulahian et al., 2008; DeLoid et al., 2009), were seeded in 96-well black-walled microscopy microplates (BD Biosciences, San Jose, CA, USA) at 100,000 cells per well in Roswell Park Medical Institute culture medium containing 10% fetal bovine serum (RPMP/10% FBS), and incubated at 37 C and 5% CO_2 for 48 hours to become adherent. ENM suspensions were prepared by probe sonicating (Sonifier Cell Disruptor, model W-200P, Branson Sonic Power Co., Plainview, L.I, NY, fitted with a 1/8" tapered microtip, operating in continuous mode at 40% power output) 10 mg of particles in 1 ml of RPMI (without serum) for 20 seconds, and diluting to final treatment concentrations in RPMI/10%FBS. Cells were incubated at 37 C and 5% CO_2 for three hours with the ENM suspensions (0.05 or 0.5mg/ml of either SiO_2 ; 1, 5 or 10% wt Ag on SiO_2 ; or 4.7 nm or 6.7 nm Fe_2O_3), washed twice with PBS, and incubated overnight in RPMI/10% FBS. Cells were then incubated for 30 minutes with 0.5 μM SYTOX Green (Invitrogen, Carlsbad, CA, USA) in Hank's balanced salt solution containing 0.3% bovine serum albumin (HBSS/0.3% BSA), washed twice with PBS, fixed with 4% formaldehyde for ten minutes, stained with 2.5 $\mu\text{g}/\text{ml}$ of the blue fluorescent cytoplasmic dye HCS CellMask Blue (Invitrogen) and 0.5 $\mu\text{g}/\text{ml}$ of the blue fluorescent nuclear stain Hoechst 33342 (Invitrogen) in HBSS for one hour at room temperature, and washed twice with PBS.

Plates were imaged using a BD Pathway 855 High Content Bioimager (BD Biosciences). Blue and green confocal fluorescence images were acquired for each well using a 20 \times NA075 objective (Olympus, Center Valley, PA, USA), and appropriate excitation, dichroic and emission filters. Image analysis was performed using custom software developed in MATLAB[®] (The Mathworks, Inc., Natick, MA, USA), and consisted of automated segmentation and identification of individual cells (from blue fluorescence images) and calculation of mean green fluorescence (indicative of membrane damage) and percentage of positive (dead) cells based on a user-selected green fluorescence image intensity threshold.

Results and Discussion

Performance characterization

VENGES's ability to generate crystalline and amorphous metal oxide nanomaterials, while controlling their particle size, was demonstrated as follows:

Generation of crystalline Fe₂O₃ nanoparticles—Figures 2 and 3 show TEM images and XRD spectra of Fe₂O₃ nanoparticles made at different liquid precursor to dispersing gas flow ratios in VENGES. The TEM images revealed the spherical nature of the primary Fe₂O₃ particles, in agreement with FSP synthesis of Fe₂O₃ (Strobel and Pratsinis, 2009; Li et al., 2006). These primary particles were linked into chain-like agglomerates with a size of tens of nanometers. As shown in the TEM images, the liquid precursor to dispersing gas flow ratio defined the size of the primary particles. Primary particles produced at a 4/6 ratio (Figure 2a) were smaller than those produced at a 7/3 ratio (Figure 2b), likely because the former experienced lower precursor concentrations and temperatures, and shorter residence times. Also, because the 4/6 flame was quenched more rapidly, particles produced at the lower ratio had less time to grow by coagulation and sintering, and thus formed smaller aggregates. Consistent with the TEM analysis, the XRD results indicate that higher precursor flow rates (and lower dispersing gas flow rates) result in the formation of larger crystal particles: the crystal size of γ -Fe₂O₃ increased from 2 nm for the 3/7 ratio to 5.8 nm for the 7/3 ratio.

Figure 4 summarizes VENGES's ability to control the particle size and SSA. Measured SSA, equivalent BET particle size (d_{BET}), and XRD estimated crystal size (d_{XRD}) are presented as a function of liquid precursor to dispersing gas flow ratio. It is worth pointing out that for all ratios, d_{XRD} is smaller than d_{BET} . This indicates a polycrystalline structure in the generated Fe₂O₃ (i.e. each nanoparticle consists of multiple crystals).

Generation of amorphous SiO₂ nanoparticles of varying particle size—TEM images of amorphous SiO₂ nanoparticles generated by the VENGES system at 3/7, 5/5, 6/4, and 7/3 precursor to dispersing gas ratios are shown in Figure 5. XRD analysis revealed the amorphous nature of SiO₂ particles, in agreement with previous studies (Ulrich, 1984). Silica nanoparticles are linked together into a chain-like agglomerate morphology with a size of tens of nanometers, similar to Fe₂O₃ nanoparticles. Measured SSA and equivalent BET particle size (d_{BET}) for SiO₂ particles, as a function of the precursor to dispersing gas ratio, are shown in Figure 6.

VENGES's ability to reproducibly generate ENMs with the same properties for the same flame conditions was tested by generating SiO₂ particles for a series of liquid precursor to dispersing gas ratios in three independent experiments per ratio. Mean measured SSA and d_{BET} are displayed as a function of precursor to dispersing gas ratio in Figure 6, with standard errors for SSA values indicated by error bars. These results show that the SSA was reproduced consistently, with an error of $\pm 5 \text{ m}^2/\text{g}$, which is typical for BET measurements.

In addition, findings shown in figures 4 and 6 are consistent with the published literature on aerosol dynamics related to the synthesis of SiO₂ and Fe₂O₃. Comparing Fig. 4 and 6 one

recognizes first that larger SiO₂ than Fe₂O₃ particles are formed reflecting the 10:1 difference in precursor concentration (Table 1). Second, the Fe₂O₃ solvent contains 50% by volume 2-EHA that favors formation of particles with uniform characteristics (Stark et al., 2003). These two differences facilitate the rapid evaporation of Fe-acetylacetonate and formation of Fe₂O₃ particles by gas-to-particle conversion. Therefore, increasing the FSP liquid precursor/gas ratio, increases the particle concentration in the gas phase from a) the increasing metal content through the increasing FSP liquid flow and b) from the decreasing gas content that prolongs the high temperature particle residence time (Pratsinis, 1998) and increases the flame height (Madler et al., 2002a: Fig. 7). Hence increasing the FSP liquid precursor/gas ratio increases aerosol concentration and flame temperature that favor aerosol coagulation and sintering that result in larger particles and smaller SSA (Figure 4).

In the case of SiO₂ synthesis, the aerosol dynamics are different. The higher boiling point of TEOS (163-167 C) than that of ethanol (78 C) favors faster evaporation of ethanol than TEOS during spray combustion. Given the high content of TEOS (1M here), it may not be easy to instantly evaporate it all from the sprayed droplets. As a result, small SiO₂ particles are formed by gas-to-particle conversion and larger ones by droplet-to-particle conversion (Madler et al. 2002b). Figure 5a nicely shows a rather bimodal particle size distribution at FSP liquid precursor/gas ratio of 3/7. As this ratio increases to 4/6, the overall enthalpy density of the flame increases as more fuel and less dispersion O₂ is provided. This favors particle formation by gas-to-particle conversion as higher temperatures are attained (Madler et al. 2002: fig. 8) so more of TEOS can evaporate, resulting in more small particles and fewer larger ones (Fig. 5b) and higher SSA (Figure 6). As the liquid precursor/gas ratio increases further, silica formation by gas-to-particle conversion dominates over the droplet-to-particle route resulting in the smallest SiO₂ particles at FSP liquid/gas ratio of 6/4 (Figure 6). Further increasing of the FSP liquid/gas ratio elicits the response of particle formation by gas-to-particle conversion at hotter flames and more concentrated aerosols as discussed with Fe₂O₃ above resulting in larger particles by faster coagulation and sintering at FSP liquid precursor/gas ratio of 7/3 (Figure 6).

The silica aerosol dynamics observed here are consistent with FSP synthesis of SiO₂ by FSP of low enthalpy content methanol or ethanol solvents exhibiting a maximum in SSA (Madler et al., 2002a: Fig. 10) as in Figure 6 here. In contrast, when high enthalpy content iso-octane solvent were used, a monotonic reduction of SSA was observed (Madler et al., 2002a: Fig. 10) as with Fe₂O₃ in Figure 4 here.

Surface modification of generated ENMs—The surface of SiO₂ nanoparticles was modified by depositing on them different mass fractions of nanosilver. The morphology of SiO₂ nanoparticles with 10% wt surface Ag nanoparticles, generated at a 5/5 liquid precursor to dispersing gas ratio, is shown in Figure 7. Ag nanoparticles are clearly shown as “bright” white spots on the surface of SiO₂ nanoparticles. The number of Ag particles as a function of size was enumerated from the STEM image in Figure 7. It is worth noting that most of the counted Ag nanoclusters are in the size range of 1-3 nm and the specific surface area of silica nanoparticles was that obtained in Figure 6 (about 255 m²/g, Table 3). Experiments started with the production of pure SiO₂ nanoparticles, followed by the surface modification experiments. For pure SiO₂, the typical amorphous reflection in XRD was

detected (Figure 8). The same reflection was also seen in the XRD spectra in the case of the surface deposition of Ag nanoparticles. With higher Ag mass fraction, stronger XRD peaks for Ag were obtained (Height et al., 2006). It should be noted that at high Ag contents (e.g. 99 wt% here), polycrystalline Ag particles are formed in contrast to the monocrystalline at 5 and 10 wt% Ag on SiO₂. The detected bulk phase was metallic Ag⁰, although AgO_x nanoparticles might also have been formed on the SiO₂ particle's surface. Our results confirm that the VENGES system can generate surface modified SiO₂ nanomaterials, and that the nanomaterial cluster size can be varied by changing both the Ag mass fraction content as well as the precursor solution.

Results from toxicological studies

Animal instillation experiments—Different liquid dispersion strategies vary in their effectiveness, and thus determine the size of agglomerates in the final suspension. These strategies may also influence the particle surface charge and reactivity (Oberdorster et al., 2007), with implications for toxicological properties. We used PBS, a common physiologic medium, combined with ultrasonic dispersion for 2 minutes. The tube containing the nanoparticle suspension was immersed in ice to absorb the heat generated during the sonication process. Immediately after sonication, the size of agglomerates was determined by dynamic light scattering (DLS). As shown in Table 3, such liquid dispersion techniques cannot break down the agglomerates to nanostructure level, because they consist of aggregates of nanoparticles with significant forces of adhesion (Teleki et al., 2008a). Nevertheless, the size of the Ag/SiO₂ particles measured by DLS (190 nm) is comparable to the roughly 120-280 nm size of commercially available flame-made silica grades (Camenzind et al., 2010). Although the specific surface areas of these two ENMs were close (298 and 255 m²/g for iron oxide and Ag/SiO₂ respectively), differences in the chemical composition resulted in different dispersions in the same medium, as has been reported for flame-made silica-titania (Teleki et al., 2008b). The iron oxide agglomerate sizes were larger (1.76 μm) than similarly dispersed 10% wt Ag/SiO₂ particles (0.19 μm). This was somewhat expected, since it is known that SiO₂ nanoparticles, because of their low iso-electric point (relative to that of pure iron oxide nanoparticles), are more easily dispersed in liquid suspensions.

Using the aforementioned dispersion strategy, we conducted a pilot experiment to test the effects of these ENMs in inducing pulmonary injury and inflammation in a rat bioassay system (Beck et al, 1982). Pulmonary responses to similarly sized iron oxide and 10% wt Ag on SiO₂ were compared. At 24 hours post-exposure, different BAL parameters of injury and inflammation in both iron oxide- and 10% wt Ag/SiO₂-instilled rats were significantly increased compared with PBS control. The total number of lavaged macrophages, lymphocytes, and eosinophils did not differ between either nanoparticle and PBS control. However, neutrophils, which are significant markers of inflammation, were significantly increased in both nanoparticle-exposed groups compared with control (Figure 9a). In addition, BAL levels of myeloperoxidase, an indicator of neutrophil degranulation, were also increased in the nanoparticle-treated rats, consistent with the neutrophil data (Figure 9b). Lactate dehydrogenase, a measure of cell death or damage, was also significantly increased. The albumin levels, a measure of capillary permeability in the lungs, were

significantly higher in both groups compared with control. The level of hemoglobin in BAL reflects the degree of alveolar hemorrhage. At a dose of 1 mg/kg, neither nanoparticle induced hemorrhage. The hemoglobin levels in all three groups were similar. BAL parameters from nanoparticle exposed rats were similar except for albumin.

Rats instilled with 10% wt Ag on SiO₂ had higher albumin levels than rats instilled with iron oxide. This difference may be due to the smaller agglomerate size in the suspension, in addition to inherent differences in physical and chemical characteristics of the two types of ENMs. Our data show that using uniformly generated and carefully characterized ENMs in toxicological studies can both elucidate quantitative responses *in vivo*, and provide testable mechanistic hypotheses for further studies. Future studies will test hypotheses such as the effects of particle agglomerate size and/or type on pulmonary responses. In addition, other animal studies will be performed to compare these results to those obtained by inhalation of freshly generated ENMs.

Membrane integrity cytotoxicity experiments—Results of the membrane integrity cytotoxicity experiments are illustrated in Figure 10 and detailed in Table 4. Both particle type- and concentration-dependent cytotoxicity were observed. SiO₂ and 1% Ag on SiO₂ particles, for example, were non-toxic at 0.05 mg/ml, but were highly toxic at 0.5 mg/ml. Both 5% and 10% Ag on SiO₂, on the other hand, caused significant membrane toxicity at the lower concentration, consistent with the high toxicity of nanosilver. Iron oxide particles (4.7 and 6.7 nm) were toxic only at the higher concentration (0.5 mg/ml).

Conclusions

A novel engineered nanomaterial (ENM) generation system for the *in situ* toxicological characterization of engineered nanoparticles within biological matrices was developed and characterized. The VENGENS system is based on industry-relevant, flame spray pyrolysis (FSP) aerosol reactors, and can be used for both *in vitro* cellular studies and *in vivo* inhalation studies. The ability of VENGENS to produce families of engineered nanomaterials of pure and selected mixtures of iron oxide, silica and nanosilver with controlled physico-chemical properties was demonstrated in laboratory characterization experiments using a range of state-of-the-art-techniques.

The VENGENS system is versatile and can be used to reproducibly generate almost any metal oxide at high production rates (g/hr). The physico-chemical properties of the generated ENMs (composition, particle size, surface, morphology) can be easily adjusted using the VENGENS system. In addition, no drying or annealing is needed to collect nanoparticles.

VENGENS's suitability for toxicological studies was demonstrated in pilot *in vitro* cellular studies and *in vivo* animal instillation experiments. Preliminary results link important physico-chemical ENM properties to toxicity. The striking particle composition and size dependence seen in pilot cytotoxicity assay results with VENGENS generated particles further support the utility of the developed system for creation of relevant bioassay-compatible nanomaterials.

Further results from the aerosol characterization and animal inhalation studies, as well as *in vitro* functional and toxicity assays, will be reported in future manuscripts. Exposing animal models *in vivo* is a very important aspect of nanotoxicology. The use of the VENGES aerosol generation system along with the development of new *in vitro* screening methodologies and *in vivo* inhalation studies will help to determine which physico-chemical properties correlate best with biointeractions.

Acknowledgments

We kindly acknowledge financial support from Harvard University, the HSPH-NIEHS Center (Grant #ES000002), and ETH Zürich (ETH Research Grant TH-09 06-2). We also thank Dr. David Bell from the Harvard Center for Nanoscale Systems for the STEM analysis, as well as Dr. Frank Krumeich (ETH) and the Electron Microscopy Center of ETH Zurich (EMEZ) for providing the necessary infrastructure for the TEM images. We thank Thomas Donaghey for technical support with the *in vivo* toxicology studies and Melissa Curran for helpful editorial suggestions and TETHIS for providing the FSP apparatus for the ENM synthesis.

References

- Aitken RJ, Chaudhry MQ, Boxall ABA, Hull M. Manufacture and use of nanomaterials: current status in the UK and global trends. *Occup Med.* 2006; 56:300–306.
- Beck BD, Brain JD, Bohannon DE. An *in vivo* hamster bioassay to assess the toxicity of particulates for the lungs. *Toxicol Appl Pharmacol.* 1982; 66:9–29. [PubMed: 6925426]
- Brain JD, Curran MA, Donaghey T, Molina R. Biologic responses to nanomaterials depend on exposure, clearance, and material characteristics. *Nanotoxicology.* 2009; 3:1–7.
- Brain JD, Godleski J, Kreyling W. *In vivo* evaluation of chemical biopersistence of nonfibrous inorganic particles. *Environ Health Perspect.* 1994; 102:119–125. [PubMed: 7882915]
- Camenzind A, Schweizer T, Sztucki M, Pratsinis SE. Structure & Strength of Silica-PDMS Nanocomposites. *Polymer.* 2010; 51:1796–1804.
- Colvin VL. The potential environmental impact of engineered nanomaterials. *Nat Biotechnol.* 2003; 21:1166–1170. [PubMed: 14520401]
- DeLoid GM, Sulahian TH, Imrich A, Kobzik L. Heterogeneity in macrophage phagocytosis of *Staphylococcus aureus* strains: high-throughput scanning cytometry-based analysis. *PLoS One.* 2009; 4(7):1–13. e6209 (OR).
- Height, MJ.; Pratsinis, SE. Antimicrobial and antifungal powders made by flame spray pyrolysis. European Patent EP1846327 (A1). 2007.
- Hilty F, Teleki A, Krumeich F, Büchel R, Pratsinis SE, Langhans W, Hurrell H, Zimmermann M. Development and optimization of iron- and zinc-containing nano-structured powders for nutritional applications. *Nanotechnol.* 2009; 20:475101. (11p).
- Langsrud S, Sundheim G. Flow cytometry for rapid assessment of viability after exposure to a quarternary ammonium compound. *J Appl Bacteriol.* 1996; 81:411–418. [PubMed: 8896352]
- Li D, Teoh W, Selomulya C, Woodward R, Amal C, Rosche B. Flame-sprayed superparamagnetic bare and silica-coated maghemite nanoparticles: Synthesis, characterization, and protein adsorption-desorption. *Chem Mater.* 2006; 18:6403–6414.
- Lu H, Khan A, Pratsinis SE, Smirniotis P. Flame-made durable doped-CaO nanosorbents for CO₂ capture. *Energy & Fuels.* 2009; 23:1093–1100.
- Lubick N. Nanosilver toxicity: ions, nanoparticles or both? *Environ Sci Technol.* 2008; 42:86178617.
- Madler L, Kammler HK, Mueller R, Pratsinis SE. Controlled synthesis of nanostructured particles by flame spray pyrolysis. *J Aerosol Sci.* 2002a; 33:369–389.
- Madler L, Stark WJ, Pratsinis SE. Flame-made Ceria Nanoparticles. *J Mater Res.* 2002b; 17:1356–62.
- Mukhopadhyay A, Basu B. Consolidation microstructure property relationships in bulk nanoceramics and ceramic nanocomposites: a review. *Int Mater Rev.* 2007; 52:257–264.
- National Research Council. Health and Safety Research. Washington D.C: The National Academies Press; 2008. Review of the Federal Strategy for Nanotechnology-Related Environmental.

- National Science and Technology Council Committee on Technology, S.o.N.S., Engineering and Technology. National Nanotechnology Initiative. Strategy for Nanotechnology-Related Environmental. Health and Safety Research. 2008
- Nel A, Madler L, Velegol D, Tian X, Eric M, Hoek V, Ponisseril S, Klaessig F, Castranova V, Thompson M. Understanding biophysicochemical interactions at the nano-bio interface. *Nat Mater*. 2009; 8:543–557. [PubMed: 19525947]
- Nel A, Xia T, Madler L, Li N. Toxic potential of materials at the nanolevel. *Science*. 2006; 311:622–627. [PubMed: 16456071]
- Oberdorster G, Stone V, Donaldson K. Toxicology of nanoparticles: A historical perspective. *Nanotoxicology*. 2007; 1:2–25.
- Pratsinis SE. Flame Aerosol Synthesis of Ceramic Powders. *Prog Energy Combust Sci*. 1998; 24:197–219.
- Roth BL, Poot M, Yue ST, Millard PJ. Bacterial viability and antibiotic susceptibility testing with SYTOX green nucleic acid stain. *Appl Environ Microbiol*. 1997; 63:2421–2431. [PubMed: 9172364]
- Service RF. Is nanotechnology dangerous? *Science*. 2000; 290:1526–1527. [PubMed: 11185512]
- Righettoni M, Tricoli A, Pratsinis SE. Si:WO₃ sensors for highly selective detection of acetone for easy diagnosis of diabetes by breath analysis. *Anal Chem*. 2010; 82:3581–3587. [PubMed: 20380475]
- Stark WJ, Madler L, Maciejewski M, Pratsinis SE, Baiker A. Flame-Synthesis of Nanocrystalline Ceria/Zirconia. *Chem Comm*. 2003; (5):588–589. [PubMed: 12669838]
- Strobel R, Pratsinis SE. Flame aerosol synthesis of smart nanostructured materials. *J Mater Chem*. 2007; 17:4743–4756.
- Strobel R, Pratsinis SE. Direct synthesis of maghemite, magnetite and wustite nanoparticles by flame spray pyrolysis. *Adv, Powder Technol*. 2009; 20:190–202.
- Sulahian TH, Imrich A, DeLoid G, Winkler AR, Kobzik L. Signaling pathways required for macrophage scavenger receptor-mediated phagocytosis: analysis by scanning cytometry. *Respir Res*. 2008; 9:59–71. [PubMed: 18687123]
- Teleki A, Pratsinis SE, Wegner K, Jossen R, Krumeich F. Flame-coating of titania particles with silica. *J Mater Res*. 2005; 20:1336–1445.
- Teleki A, Wengeler R, Wengeler L, Nirschl H, Pratsinis SE. Distinguishing between aggregates and agglomerates of flame-made TiO₂ by high pressure dispersion. *Powder Technol*. 2008a; 181:292–300.
- Teleki A, Akhtar MK, Pratsinis SE. The Quality of SiO₂ Coatings on flame-made TiO₂ -based Nanoparticles. *J Mater Chem*. 2008b; 18:3547–3555.
- Teleki A, Heine MC, Krumeich F, Akhtar MK, Pratsinis SE. In situ coating of flame-made TiO₂ particles with nanothin SiO₂ films. *Langmuir*. 2008c; 24:12553–12558. [PubMed: 18850688]
- Teleki AM, Suter M, Kidambi P, Ergeneman O, Krumeich F, Nelson B, Pratsinis SE. Hermetically coated superparamagnetic Fe₂O₃ particles with SiO₂ nanofilms. *Chem Mater*. 2009; 21:2094–2100.
- Teleki A, Bjelobrck N, Pratsinis SE. Continuous surface functionalization of flame-made TiO₂. *Langmuir*. 2010; 26:5815–5822. [PubMed: 20192157]
- Tsantilis S, Pratsinis SE. Soft- and hard-agglomerate aerosols made at high temperatures. *Langmuir*. 2004; 20:5933–5947. [PubMed: 16459612]
- Ulrich GD. Flame synthesis of fine particles. *Chem Eng News*. 1984; 62(22):22–29. [PubMed: 11541976]
- Wegner K, Pratsinis SE. Scale-up of nanoparticle synthesis in diffusion flame reactors. *Chem Eng Sci*. 2003a; 58:4581–4589.
- Wegner K, Pratsinis SE. Nozzle-quenching process for controlled flame synthesis of titania nanoparticles. *AIChE J*. 2003b; 49:1667–1679.

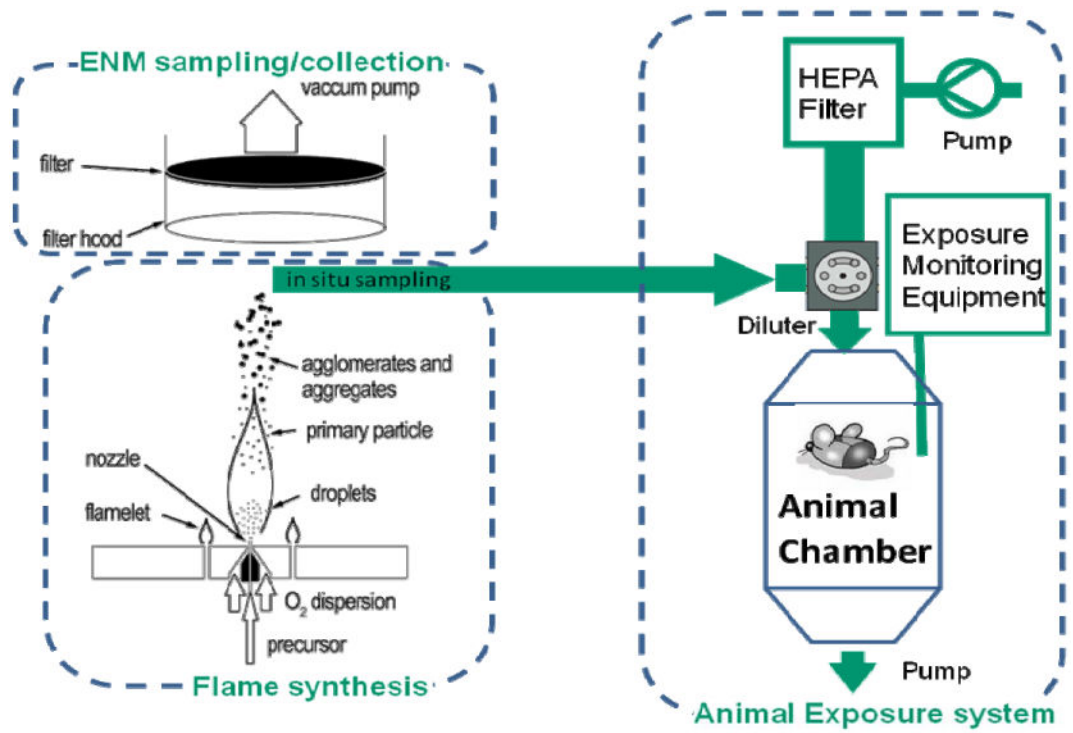


Figure 1.
Schematic diagram of the VENGES system.

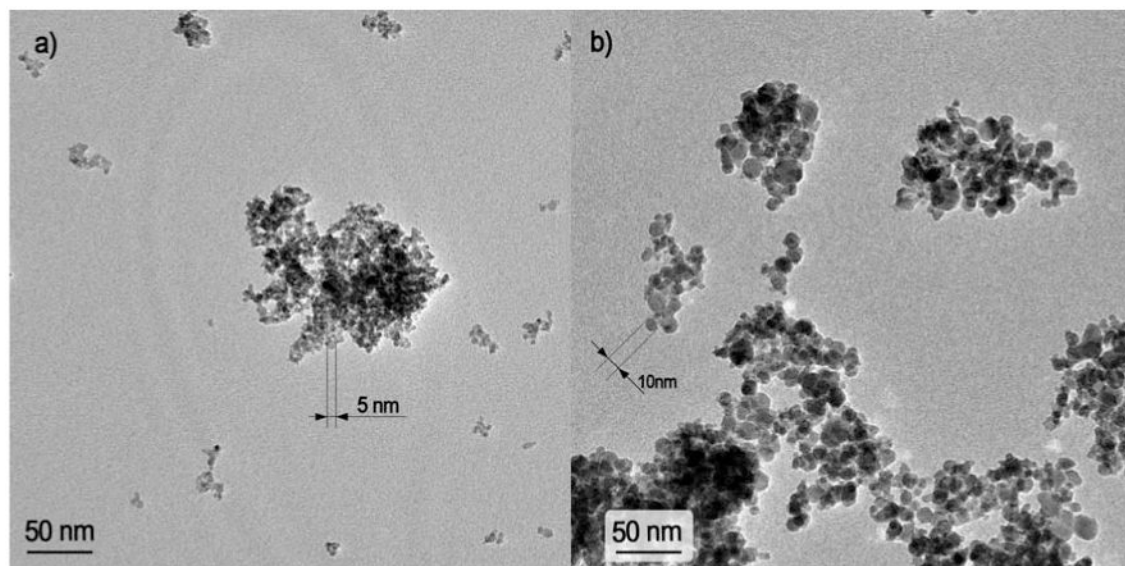


Figure 2. TEM images of Fe_2O_3 nanoparticles generated at different liquid precursor to dispersing gas ratios: a) 4/6 ratio, b) 7/3 ratio.

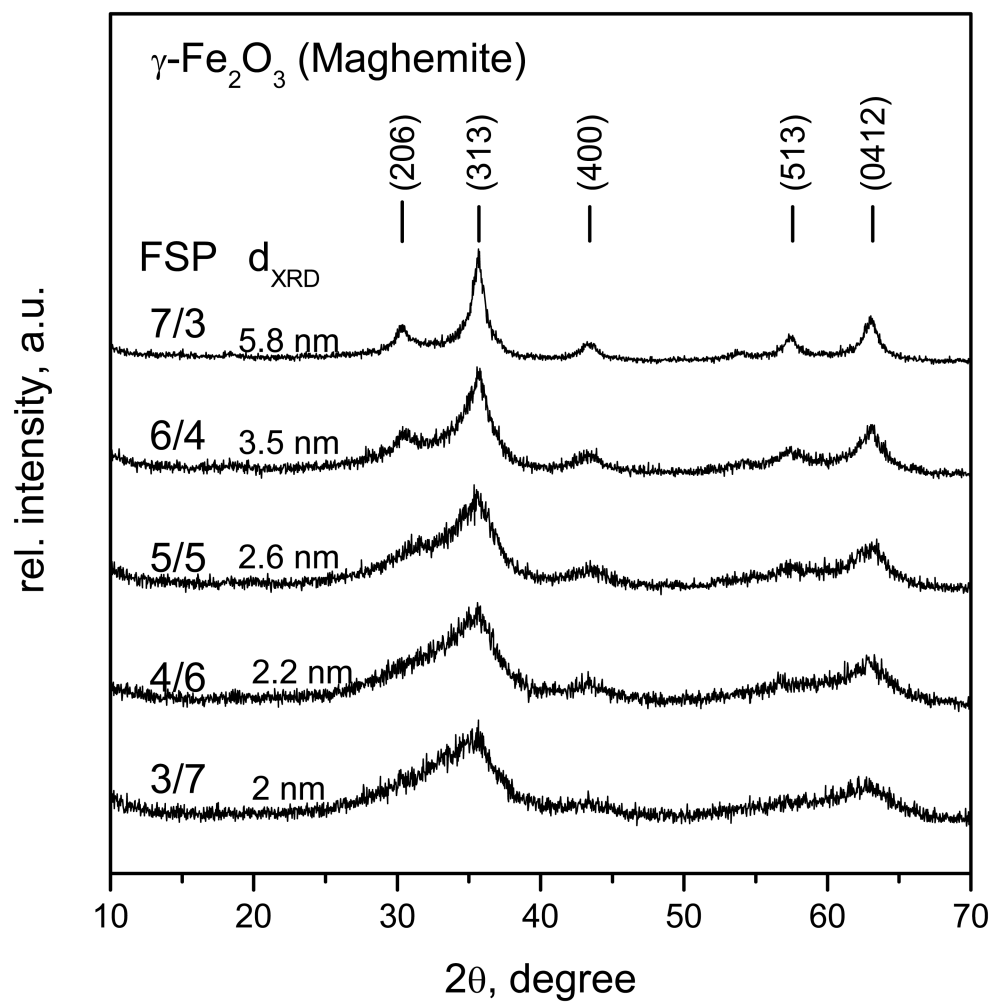


Figure 3. XRD spectra for ($\gamma\text{-Fe}_2\text{O}_3$) nanoparticles for different liquid precursor to dispersing gas ratios (Miller indices, hkl, according to the ICSD 8721 are indicated in parentheses)

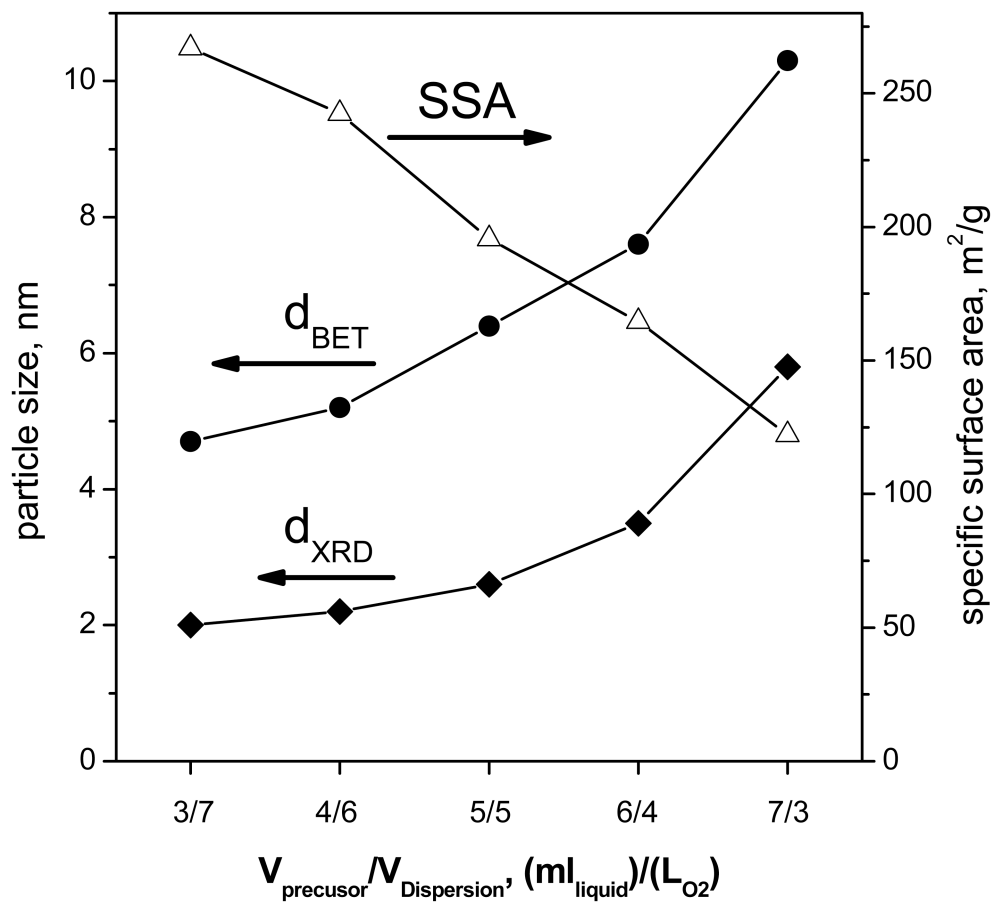


Figure 4. Fe_2O_3 specific surface area (SSA) (triangles), corresponding particle diameter (d_{BET} , circles), and crystal size (d_{XRD} , diamonds) as a function of FSP liquid precursor to dispersion O_2 flow ratio. Increasing ratios increase particle concentration and high temperature particle residence time resulting in large primary particles and crystals.

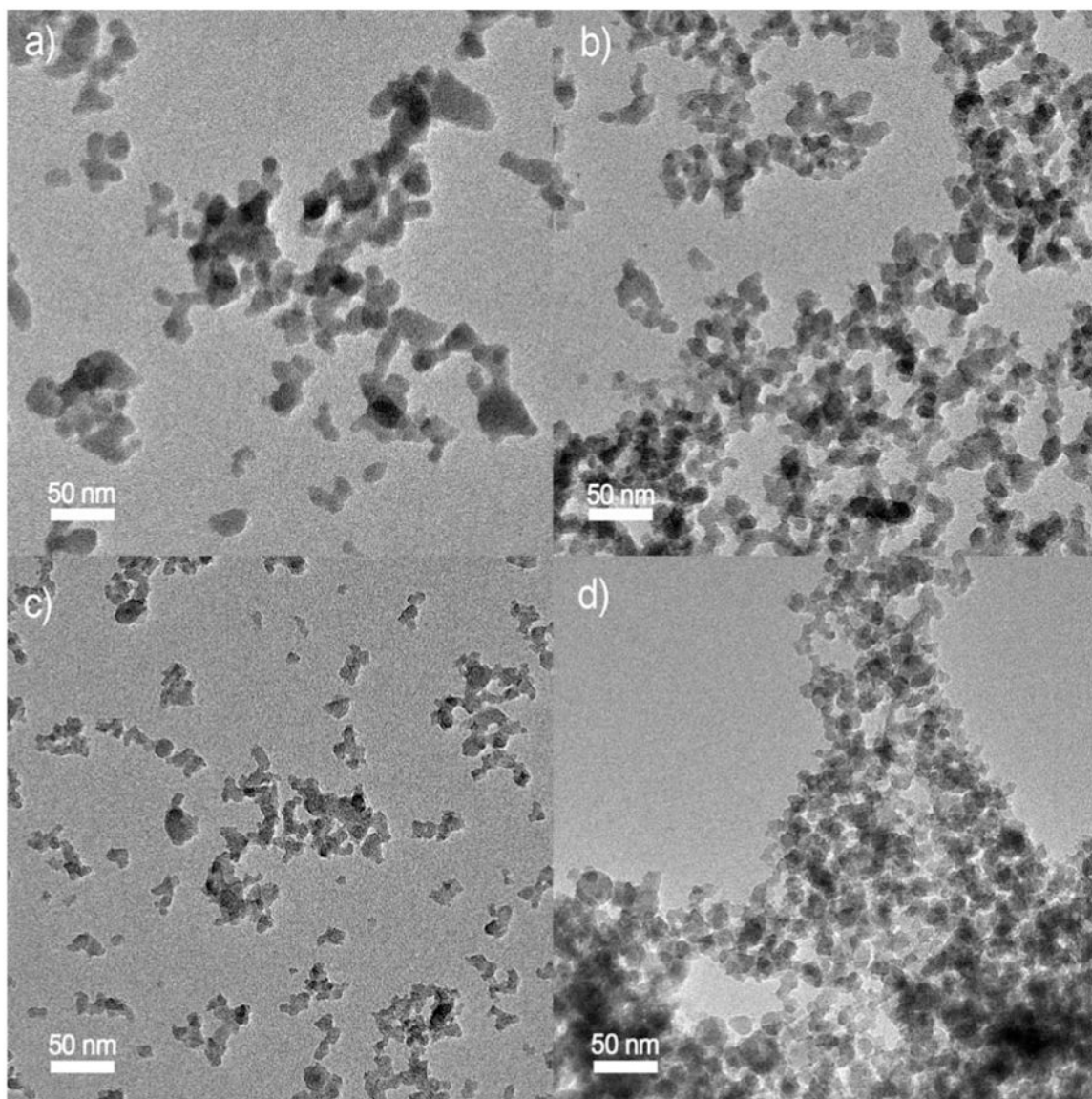


Figure 5.
SiO₂ TEM images at different liquid precursor to dispersing O₂ flow ratios: a) 3/7, b) 5/5, c) 6/4, and d) 7/3.

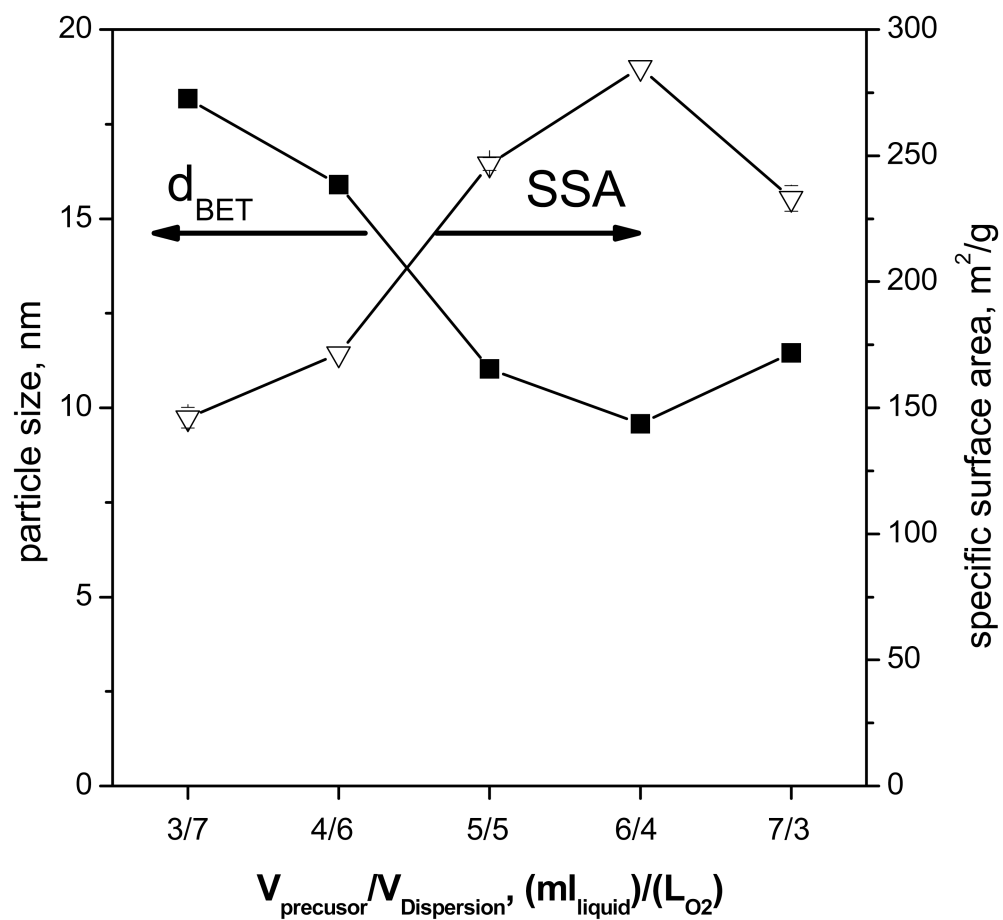


Figure 6. SiO₂ specific surface area (SSA, triangles) and the corresponding particle diameter (d_{BET} , squares) as a function of FSP liquid precursor to dispersion O₂ flow ratio.

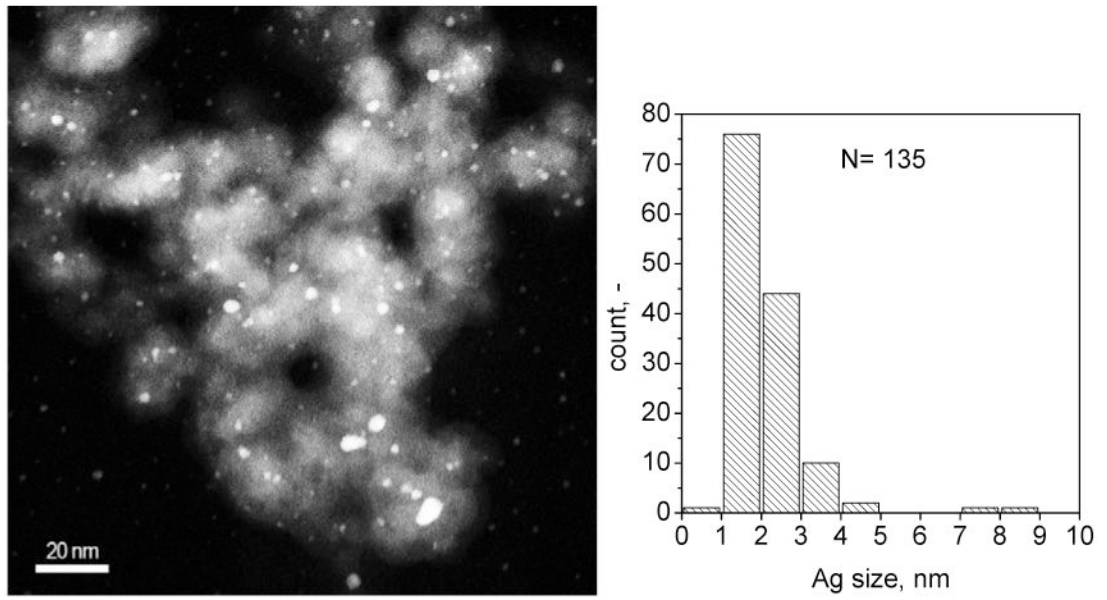


Figure 7.
STEM image of 10% Ag on SiO₂ and the corresponding Ag particle size distribution.

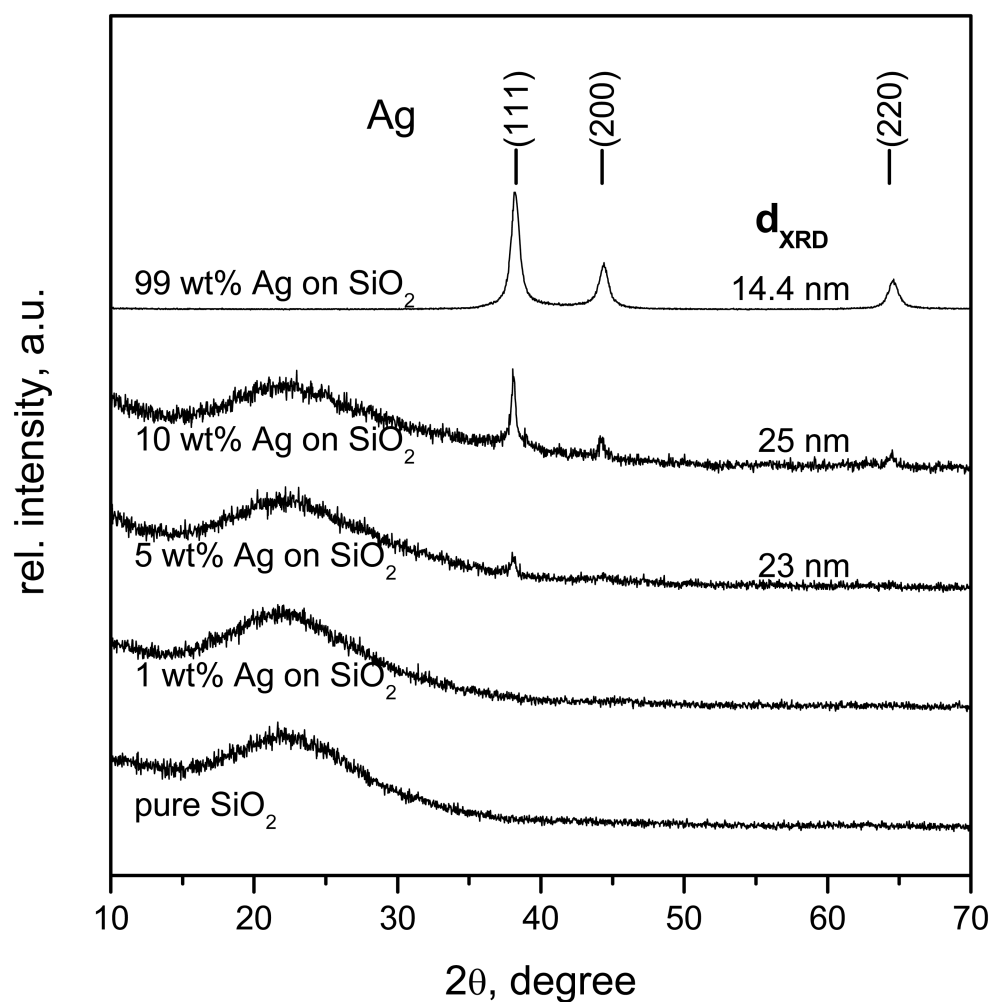


Figure 8. XRD of Ag deposited on the surface of SiO₂ nanoparticles for different % wt of Ag. The d_{XRD} size of silver is indicated that comes mostly from the large mode of bimodal Ag size distribution arising from FSP of Ag nitrate solutions (Heine and Pratsinis, 2007). In parenthesis the Miller indices (hkl) of the crystal planes according to the ICSD 64997 is indicated.

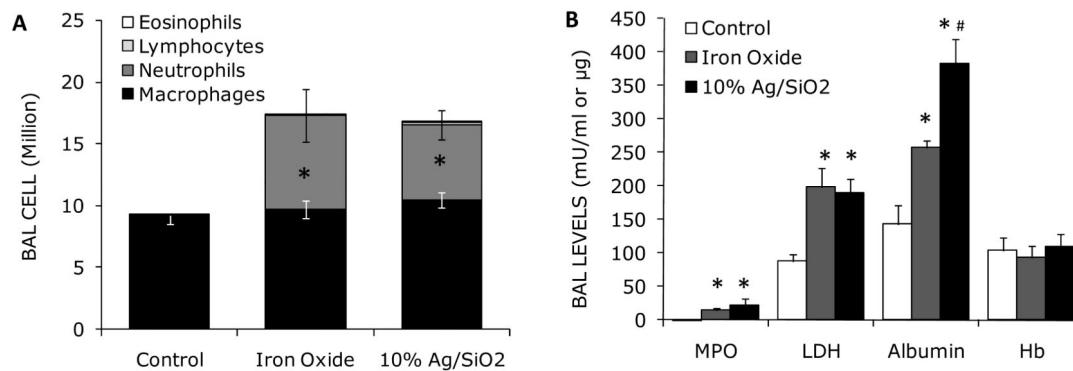


Figure 9.

Cellular and biochemical parameters of lung injury and inflammation. A. Differential cell counts in BAL at 24 hours post-exposure. There were significant increases in lavaged neutrophils when rats were instilled with 1 mg/kg iron oxide or 10% wt Ag on SiO₂. B. Biochemical parameters of injury/inflammation. Instillation of suspension of iron oxide (D_{DLS} 1.76 µm) or 10% wt Ag on SiO₂ (D_{DLS} 0.19 µm) significantly increased myeloperoxidase (MPO), lactate dehydrogenase (LDH) and albumin compared with control. No significant change was observed in BAL hemoglobin levels. In addition, 10% wt Ag on SiO₂ induced higher albumin levels compared with iron oxide. (* P < 0.05, vs. control, * P < 0.05, # iron oxide vs. 10% wt Ag on SiO₂).

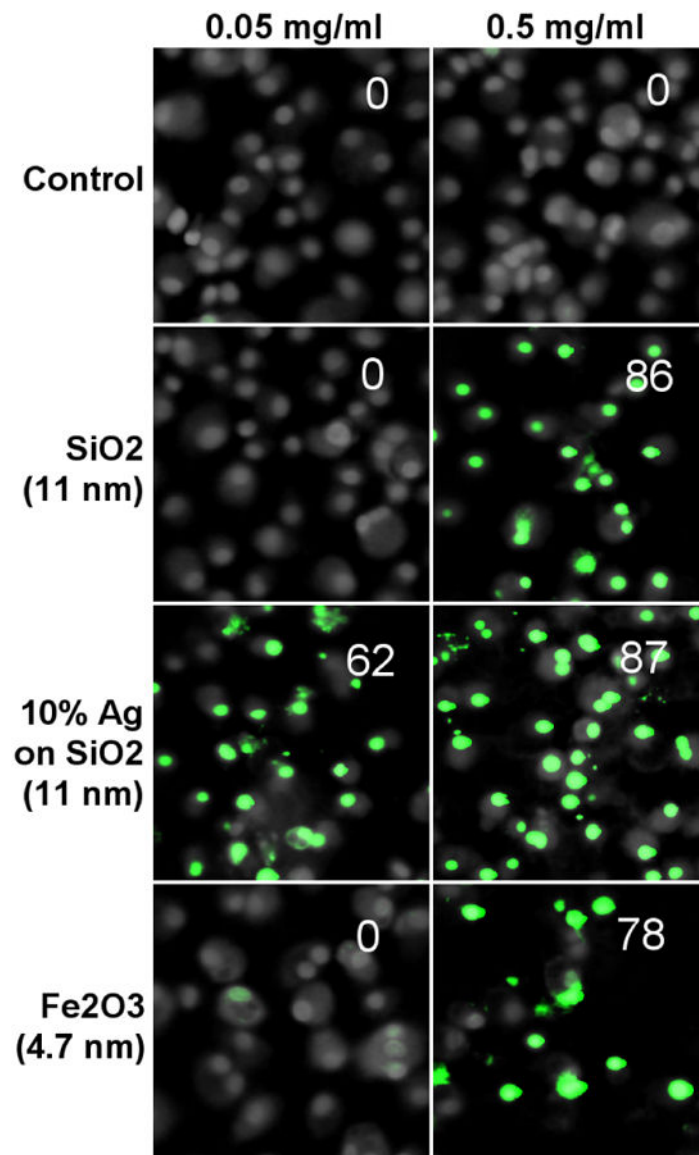


Figure 10. Membrane integrity cytotoxicity assay for 0.05 or 0.5 mg/ml solutions of sonicated ENMs. The images show particle and concentration dependent toxicity as green nuclear fluorescence; the mean % positive cells is indicated within each image.

Table 1
Engineered nanomaterial synthesis – Liquid precursor composition for synthesis of Fe₂O₃, SiO₂, and Ag supported on SiO₂

Material	Metal precursor	Solvent	Concentration (mol _{Metal} /L _{solvent})
Fe ₂ O ₃	iron(III)-acetylacetonate	ethanol and 2-ethyl-hexanoic acid 1:1 vol ratio	0.1
SiO ₂	tetraethylortho-silicate	ethanol	1
1-10 wt% Ag on SiO ₂	tetraethylortho-silicate and silver nitrate	Ethanol (100)	1
99 wt% Ag on SiO ₂		Ethanol (66.7%) Xylene (26.6%) Water (6.7%)	0.36

Table 2
FSP conditions used to produce nanoparticles of different sizes

Flame condition (Liquid/gas flow)	Liquid precursor flow mL/min	Dispersion gas flow (O ₂) L/min	Pressure drop bar
3/7	3	7	0.9
4/6	4	6	1.8
5/5	5	5	1.9
6/4	6	4	1.3
7/3	7	3	1

Author Manuscript

Author Manuscript

Author Manuscript

Author Manuscript

Table 3
Characteristics of ENMs used in animal instillation experiments

ENM	SSA(m ² /g)	D _{DLS} (µm)
Fe ₂ O ₃	298.70	1.76
10% Ag on SiO ₂	254.64	0.19

Author Manuscript

Author Manuscript

Author Manuscript

Author Manuscript

Table 4
Membrane toxicity results

Particle (d _{BET})	Concentration (mg/ml)	Mean GFL	% Positive cells
Control	-	18.75	0.00
SiO ₂ (11nm)	0.05	15.05	0.00
	0.50	72.26	86.96
1% Ag on SiO ₂ (11nm)	0.05	17.41	0.00
	0.50	88.59	87.39
5% Ag on SiO ₂ (11nm)	0.05	61.28	62.79
	0.50	86.45	98.28
10% Ag on SiO ₂ (11nm)	0.05	55.78	62.75
	0.50	65.97	87.50
Fe ₂ O ₃ (4.7nm)	0.05	23.28	0.00
	0.50	93.66	78.95
Fe ₂ O ₃ (6.7 nm)	0.05	24.83	0.00
	0.50	61.69	60.00